Volume 19
Number 35
21 September 2021
Pages 7487-7726

Organic & Biomolecular Chemistry

rsc.li/obc

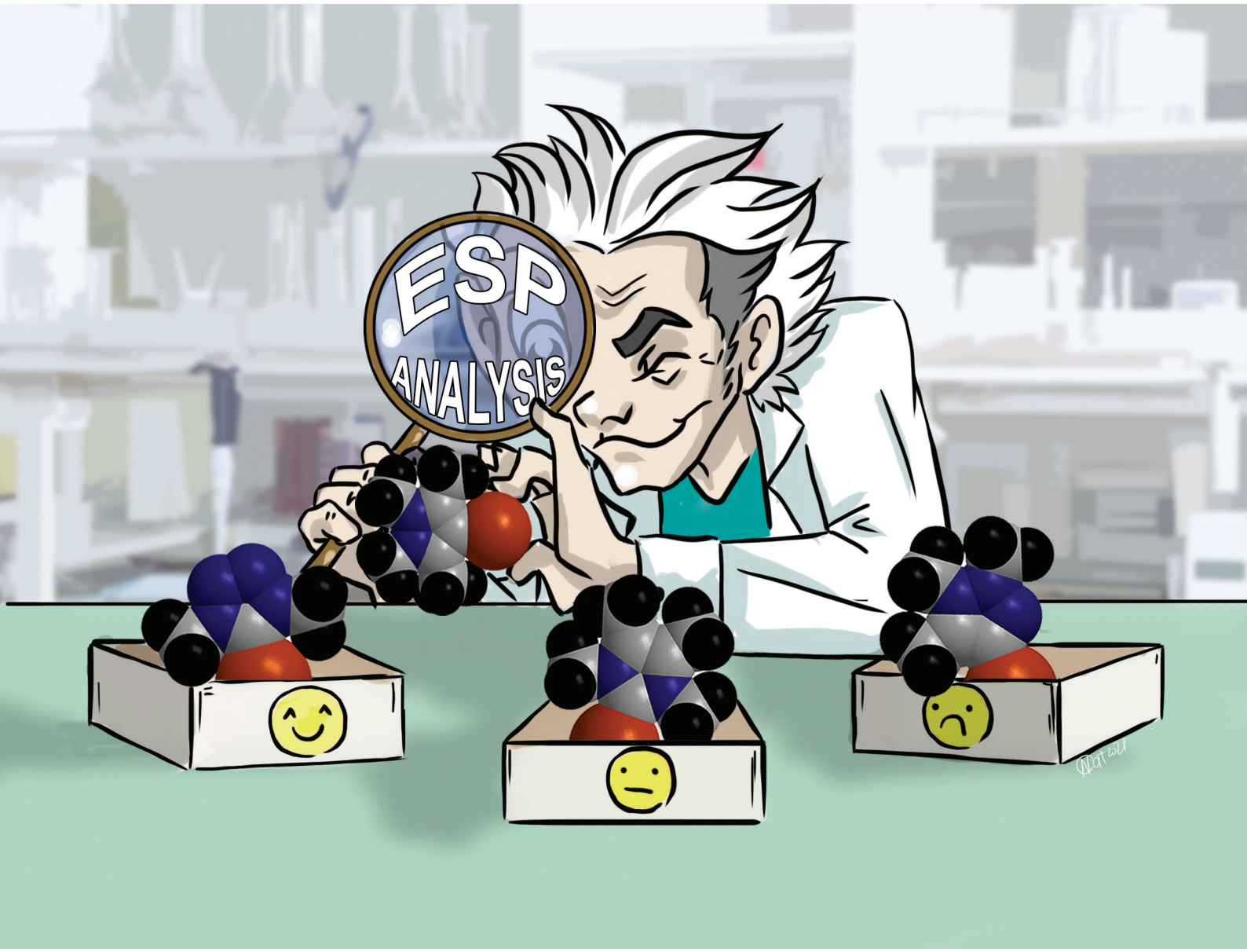

ISSN 1477-0520

ROYAL SOCIETY OF CHEMISTRY

PAPER
Dmitrii S. Bolotin *et al.*
Predicting the catalytic activity of azolium-based halogen bond donors: an experimentally-verified theoretical study

Organic & Biomolecular Chemistry

ROYAL SOCIETY OF CHEMISTRY

PAPER

View Article Online
View Journal | View Issue

Cite this: *Org. Biomol. Chem.*, 2021, **19**, 7611

Predicting the catalytic activity of azolium-based halogen bond donors: an experimentally-verified theoretical study†

Alexandra A. Sysoeva, Alexander S. Novikov, Mikhail V. Il'in, Vitalii V. Suslonov and Dmitrii S. Bolotin *

Received 15th June 2021,
Accepted 17th July 2021

DOI: 10.1039/d1ob01158h

rsc.li/obc

This report demonstrates the successful application of electrostatic surface potential distribution analysis for evaluating the relative catalytic activity of a series of azolium-based halogen bond donors. A strong correlation (R^2 > 0.97) was observed between the positive electrostatic potential of the σ-hole on the halogen atom and the Gibbs free energy of activation of the model reactions (*i.e.*, halogen abstraction and carbonyl activation). The predictive ability of the applied approach was confirmed experimentally. It was also determined that the catalytic activity of azolium-based halogen bond donors was generally governed by the structure of the azolium cycle, whereas the substituents on the heterocycle had a limited impact on the activity. Ultimately, this study highlighted four of the most promising azolium halogen bond donors, which are expected to exhibit high catalytic activity.

Introduction

Over the last decade, substantial research efforts have been focused on investigating new types of organocatalysts owing to their significant advantages over organometallic and coordination catalysts, including low to negligible sensitivity to air and moisture, reduced environmental footprint, and lower toxicity.[1,2] In general, organocatalysts can participate in either covalent or noncovalent bonding interactions with a substrate in order to promote a chemical reaction. The former activation mode involves the formation of one or several covalent bonds between the catalyst and a reaction substrate. Typically, heterocyclic carbenes,[1,3,4] amines,[1,2,5,6] and phosphines[7] comprise this type of organocatalyst. The latter activation mode involves noncovalent interactions between the catalyst and a substrate, and this type of reactivity is investigated in the present work.[2,8–12]

An organocatalyst interacting with a substrate *via* noncovalent interactions typically does so through hydrogen bonding (HB), so the use of HB donors, such as ureas,[13–18] squaramides,[18–20] and other Brønsted acids,[21–23] has led to numerous important advancements in the field of organocatalysis. In addition, noncovalent interactions can be realized *via* halogen[8–10,24–27] or chalcogen[27–29] bonding interactions (XB and ChB, respectively), but this type of catalytic activity has not been widely explored. Recent progress in the field of XB-donor catalysis has clearly indicated that cationic iodine(I)- and iodine(III)-containing species have promising potential in terms of organocatalysis owing to their high catalytic activity and remarkable stability under the necessary reaction conditions.

It has been demonstrated that 2-iodoimidazolium[10,30–32] and 4-iodo-1,2,3-triazolium[10,33–36] salts effectively catalyze an extensive series of organic transformations, including (aza)-Diels–Alder cycloadditions, Michael additions, halide abstractions, olefin reductions, and many other reactions.[10] It is worth mentioning that one report also describes the preparation of 5-iodo-1,2,4-triazolium salts and presents their catalytic activity for Michael additions.[37] Recently, hypervalent iodine(III) derivatives (*i.e.*, diaryliodonium salts) have been successfully employed for the living cationic polymerization of olefins,[38] halide abstractions,[39] and carbonyl activations.[39–41] Although diaryliodonium salts demonstrate comparable or greater organocatalytic activity than azolium-based iodine(I) derivatives for the studied reactions,[39] currently, the latter remains to be the most commonly studied type of XB-donating organocatalyst.

Considering the high catalytic activity and chemical stability of iodine(I)-containing azolium derivatives and the relatively small number of corresponding catalyst types (only three types among 14 possible variations: 2-iodoimidazoilums, 4-iodo-1,2,4-triazoliums, and to a lesser extent, 5-iodo-1,2,4-triazoliums), in this work, we aimed to estimate the potential of all structural types of iodine-containing azolium salts for

Institute of Chemistry, Saint Petersburg State University, Universitetskaya Nab. 7/9, Saint Petersburg, 199034, Russian Federation. E-mail: d.s.bolotin@spbu.ru

† Electronic supplementary information (ESI) available. CCDC 2085430–2085432. For ESI and crystallographic data in CIF or other electronic format see DOI: 10.1039/d1ob01158h

applications as XB-donating organocatalysts. Thorough quantum-chemical calculations were carried out and verified based on experimental kinetic studies.

Results and discussion

In the first stage of this work, limitations were established regarding the range of substrates to be studied. Although high catalytic activity is a key feature of any catalyst, other characteristics, such as chemical stability and synthetic accessibility also play important roles when selecting an appropriate catalyst. Therefore, iodoazoliums with N–I moieties were excluded from this study because such compounds are subject to homolytic cleavage of this bond, which may induce a series of radical or oxidative transformations. Considering the importance of chemical stability, all oxazolium derivatives were also excluded because the high electrophilicity of these compounds rendered them unstable to reactions with common nucleophiles, including H_2O.[42–45] Overall, fourteen structural types of iodoazoliums were evaluated in this study while keeping within these limitations (Fig. 1). The pentazoliums were excluded because of the absence of the C atoms in the heterocycle (only N–I bonds could be formed) and its general instability under ordinary conditions.

A review of the relevant literature data indicated that all of iododiazoliums (**A–D**) are known, but only **C** has been applied for XB-donating organocatalysis.[46–50] The diazoliums **A** and **D** served as precursors for the preparation of mesoionic carbene metal complexes by the Huynh[51–54] and Bera[55–57] groups, respectively. There is only one reported example of a type-**B** compound (*i.e.*, 1,2-dimethyl-3-iodoindazoium iodide), and its potential applications have not yet been explored. The triazoliums **E**[33,34,36,58,59] and **H**[37] were successfully utilized as organocatalysts, but no articles describe the preparation and application of compounds **F**, **G**, **I**, or **J**. The iodine-containing tetrazoliums **K–N** are also generally unexplored, and only one example of such compounds (*i.e.*, 5-iodo-1,3-diphenyltetrazolium tetrafluoroborate; type **K**) has been reported.[60] However, the catalytic properties of this compound were not studied, although it demonstrated reactivity toward a malonodinitrile anion to give phenylcyanamide (63%) and PhNHN=C(CN)$_2$ (54%).[60]

Electrostatic surface potential distribution analysis

The electrostatic potentials on the surfaces of cations (in particular, in halonium cations[61]) are entirely positive, but anisotropic. The electrostatic surface potential (ESP) distributions[62–64] were calculated for all structural types of investigated azoliums **A–N**, where all R groups were considered as methyl moieties (**A*–N***; Fig. 2). The highest potentials (V_s(max)) on the σ-holes of the I atoms fell in the range, 384–541 kJ mol^{-1}, with the cations of the studied azolium types **C***, **E***, and **H*** fell within the narrow range of moderate values (441–457 kJ mol^{-1}). With the exception of **A***, the quantity of N atoms vicinal to the I atom did not have a clear effect on the V_s(max) of the σ-holes on the I atom because of the overlap of the corresponding values (408–461 *vs.* 441–541 kJ mol^{-1} for 1N and 2Ns, respectively). Additionally, V_s(max) did not directly depend on the overall quantity of N atoms in the cycle (2Ns = 384–457; 3Ns = 408–493; 4Ns = 441–541 kJ mol^{-1}).

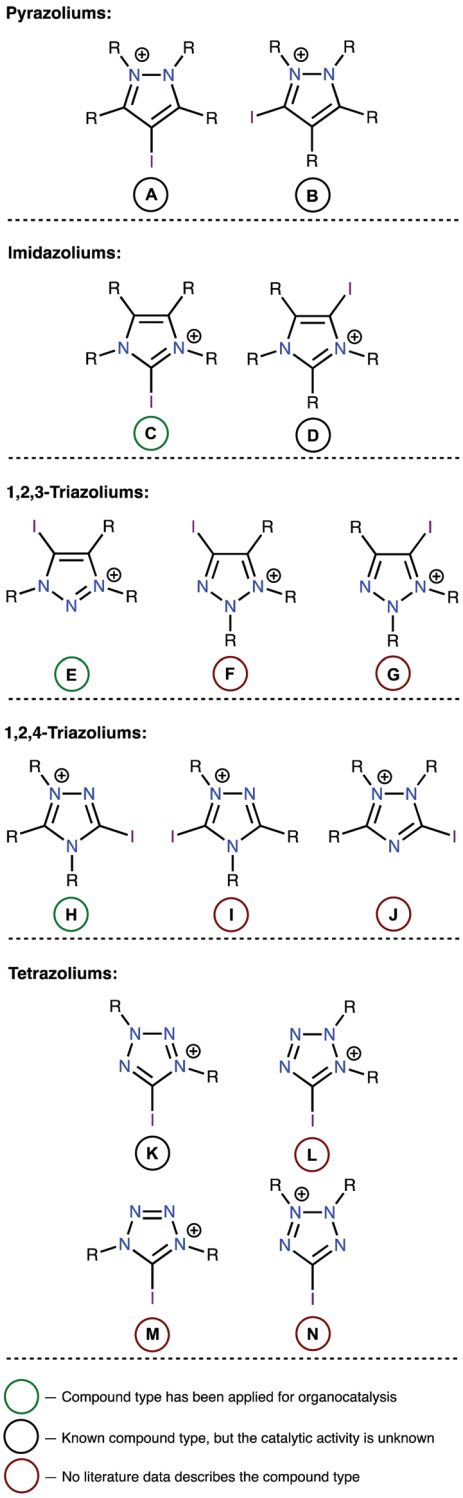

Fig. 1 Structures of the studied iodoazoliums.

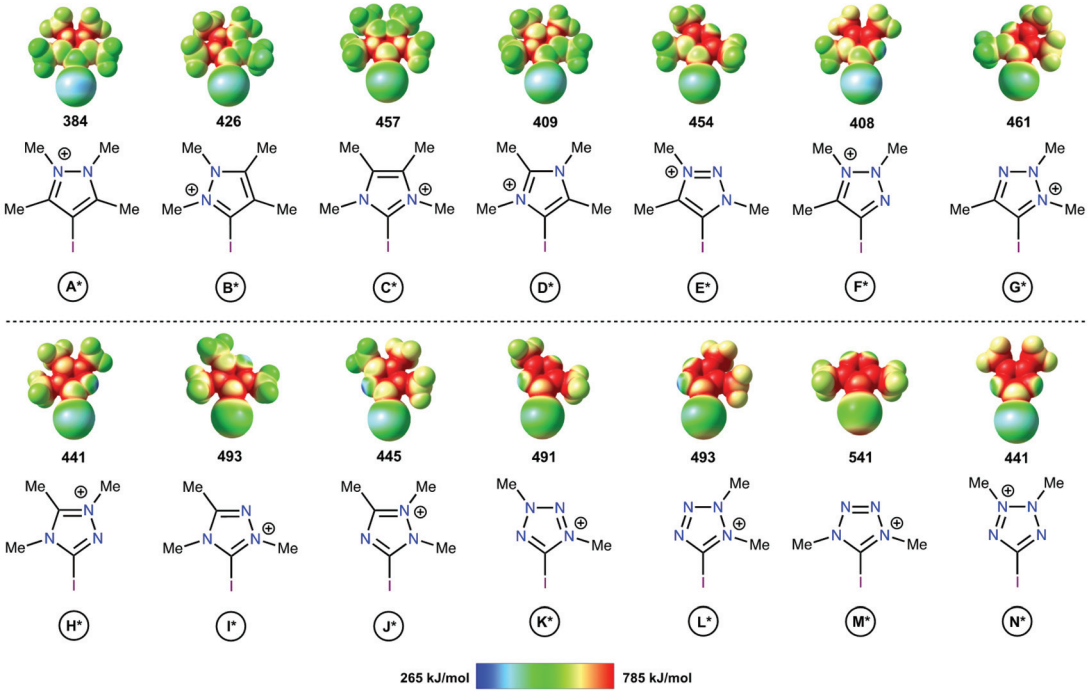

Fig. 2 Electrostatic surface potential distributions for the investigated azoliums featuring methyl substituents. The highest potentials on the iodine atom σ-hole are given in kJ mol^{-1}.

Although it is reasonable to assume that the availability of a lone pair of electrons at the vicinal position to the I atom (as in **F***, **H***, **J***, **K***, **L***, and **N***) may decrease the V_s(max) of the σ-hole, no such relationship was observed. Overall, analysis of the ESP distributions indicated that the V_s(max) of the I atom σ-hole had no appreciable dependence on a series of structural parameters of the azoliums.

Density functional theory calculations

As with other catalysts, the catalytic effect of XB donors originates from decreasing the Gibbs free energy of activation and linear free energy relationships (LFERs) between halogen bonding association constants and calculated electrostatic potentials have been documented previously.[65–67] LFERs between catalytic activity and halogen bonding association constants also have been observed.[46,68] Therefore, this phenomenon was the basis for the density functional theory (DFT) calculations carried out in this study to determine the activation energies of model reactions involving **A*–N***. The hydrolysis of methyl chloride (TS1) and the coupling of ammonia and acetone (TS2) were chosen as simple model reactions (Scheme 1 and Table 1) because XB donors have typically been studied in reactions that either required elimination of a halogen atom or carbonyl activation.[10]

The theoretical data revealed a strong correlation between the V_s(max) of the I atom σ-holes and the activation energies of the model reactions (Scheme 1 and Table 1). This suggested that the V_s(max) value may represent the relative catalytic activity of the studied azoliums. Furthermore, these results highlighted promising structural types for designing and preparing effective organocatalysts, thus also indicating which less active cation types could be disregarded.

Analysis of the V_s(max) values revealed that four azolium compounds (**I***, **K***, **L***, and **M***) featured significantly more electropositive I atoms than all other studied cation types; correspondingly, this analysis suggested that pyrazolium **A*** should be the least catalytically active among all the studied azoliums. To verify this DFT-based conclusion, a series of azoliums with unknown catalytic activities were synthesized, and kinetic measurements were carried out to study their catalytic potential. To achieve adequately representative results, the azolium types that were predicted to potentially exhibit outstanding catalytic activity were selected for these experimental investigations. Considering that the azolium types **I**, **L**, and **M** are yet unknown, and **K** is represented by only one example in the literature,[60] the synthesis and evaluation of these compounds' reactivities deserve individual in-depth studies. Therefore, pyrazoliums of type-**A** were chosen as model substrates for experimental verification of the theoretical data because relevant general synthetic strategies for their preparation were available in the literature and they demonstrated suitable stability under ordinary conditions.

Experimental confirmation of the relative catalytic activity of the studied azoliums

The pyrazolium-triflate salts [**1–5**]OTf (Scheme 2 and Fig. 3) have not been characterized previously, so they were fully characterized in the current study. Furthermore, their catalytic

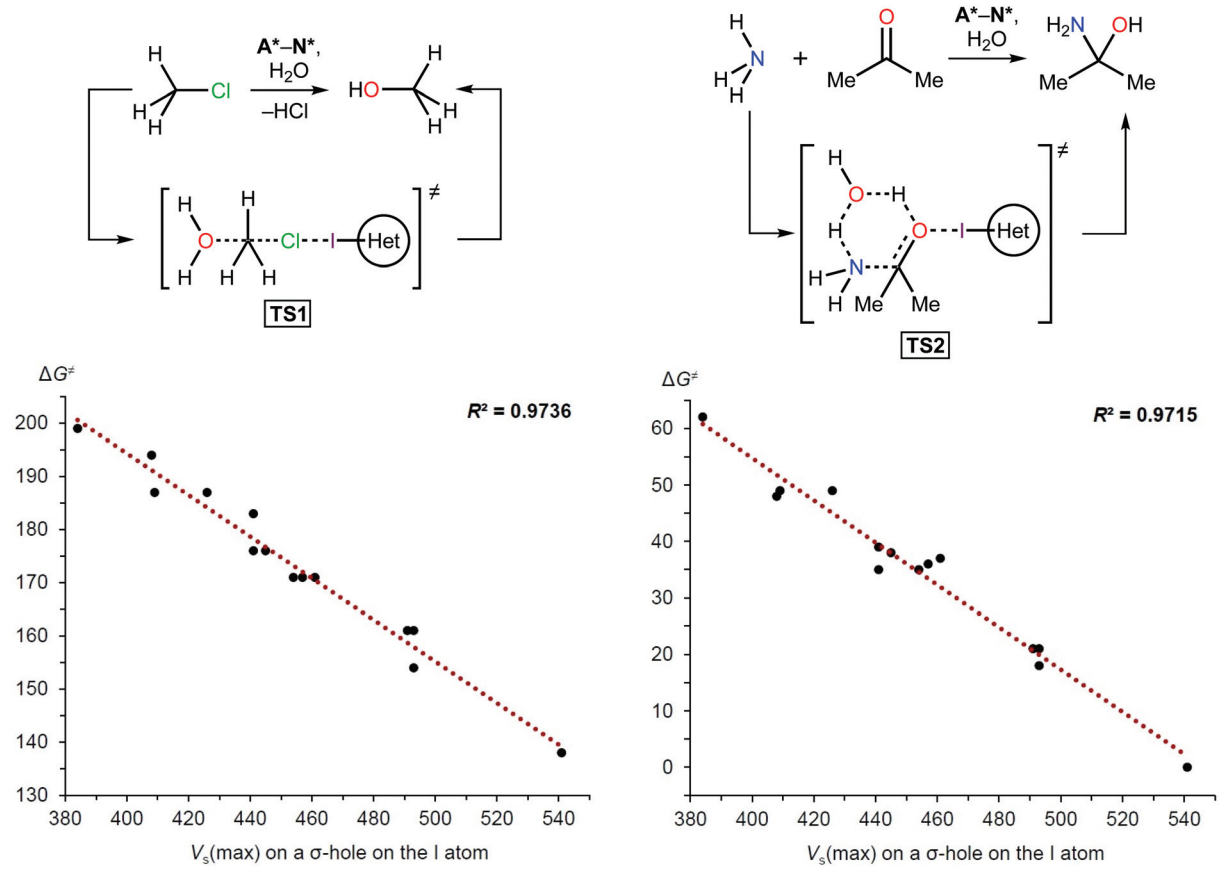

Scheme 1 Model reactions (top) and plots showing the correlation between the Gibbs free energy of activation ($\Delta G^{\neq}$; kJ mol^{-1}) and V_s(max) on the I atom σ-hole (kJ mol^{-1}).

Table 1 Calculated Gibbs free energies of activation for the modeled reactions and V_s(max) of the σ-hole on the I atom of azoliums **A*–N***

Azolium type	V_s(max) on the I atom (kJ mol^{-1})	$\Delta G^{\neq}$ (kJ mol^{-1})	
		TS1	**TS2**
A*	384	199	62
F*	408	194	48
D*	409	187	49
B*	426	187	49
N*	441	183	39
H*	441	176	35
J*	445	176	38
E*	454	171	35
C*	457	171	36
G*	461	171	37
K*	491	161	21
I*	493	161	21
L*	493	154	18
M*	541	138	0

activities were compared with the reactivities of the most abundant azolium-based organocatalysts, *i.e.*, 2-iodoimidazolium and 4-iodo-1-alkyl-1,2,3-triazolium species ([**6**]OTf and [7]OTf, respectively). The generation of 1-benzoyl-3,5-dimethylpyrazole from acetyl acetone and benzoyl hydrazide (Knorr-type reaction; Scheme 2) was selected as the model reaction for the experimental confirmation of the theoretical data because it involved carbonyl activation and was deemed suitable in our group's previous study regarding the catalytic activity of iodine (III) derivatives.[41]

Proton nuclear magnetic resonance (^{1}H-NMR) monitoring indicated that the most active species for the test reaction was the triazolium [7]OTf, and the imidazolium [**6**]OTf was less active (Fig. 4). However, a comparison of the kinetic curves of [**6**]OTf and [7]OTf within the first 30 min of the reaction indicated similar or even higher catalytic activity of [**6**]OTf. This observation suggests possible degradation of [**6**]OTf during the reaction or its inhibition by competitive binding with the product. Huber and co-workers reported similar observations in terms of the kinetics of 2-iodoimidazoliums catalyzing the Mukaiyama reaction.[50] The shape of the kinetic curves for [**6**]OTf and [7]OTf are entirely consistent with the theoretical data, *i.e.*, their nearly identical V_s(max) of the I atom σ-holes (454 and 457 kJ mol^{-1} for **E*** and **C***, respectively).

As expected, following the theoretical calculations, the pyrazoliums [**1**–**5**]OTf were significantly less active in the studied reaction, relative to the imidazolium [**6**]OTf and triazolium [7]OTf compounds, and their catalytic activities did not depend strongly on the nature of substituents on the hetero-

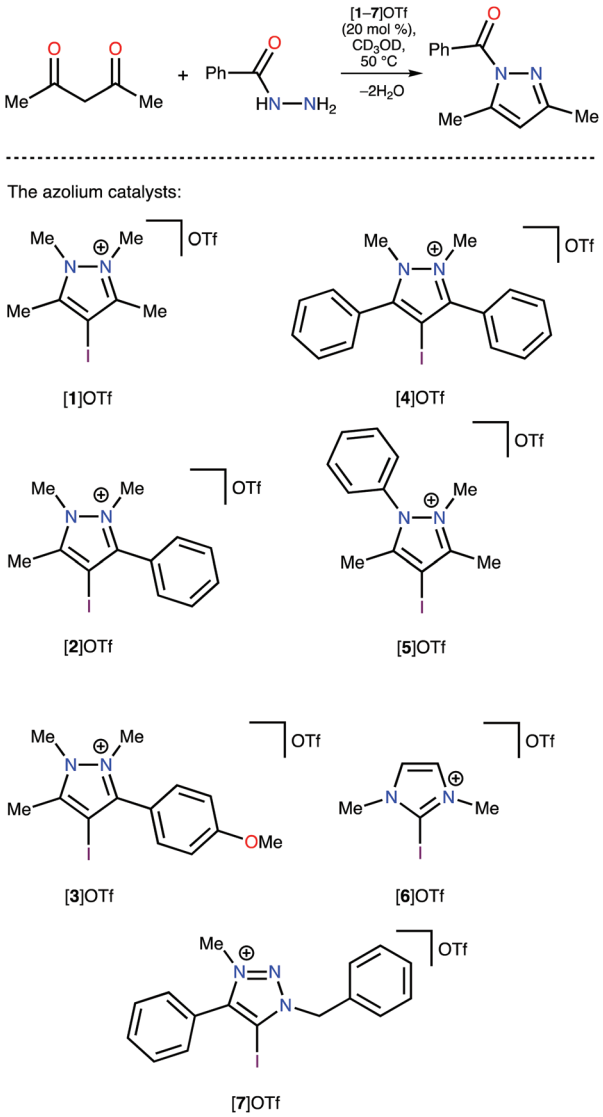

Scheme 2 The series of azolium catalysts tested in the Knorr-type reaction.

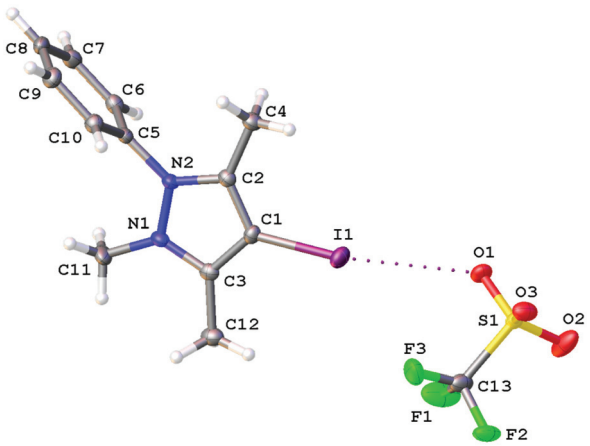

Fig. 3 The molecular structure of [5]OTf determined by X-ray diffraction.

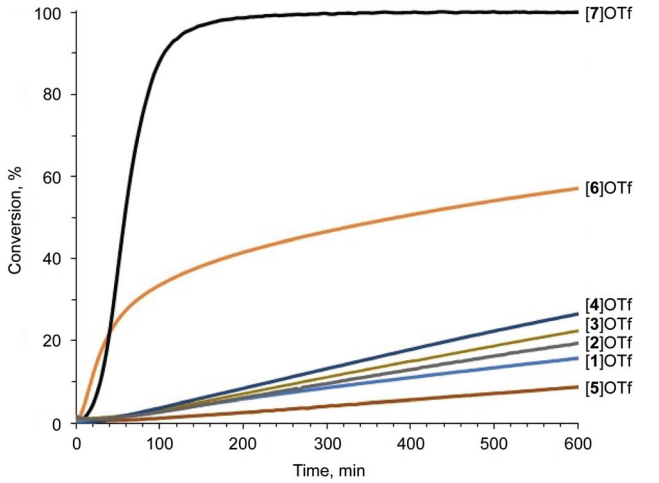

Fig. 4 Knorr-type reaction catalytic conversion based on ^{1}H-NMR monitoring. The S-shape of the kinetic curves is caused by the initial accumulation of the intermediate.[41]

cyclic system. The catalytic activity was enhanced slightly by changing the methyl groups to phenyl moieties, which exhibited weaker electron donating effects at the vicinal position relative to the I atom ([**1**–**4**]OTf); however, activity decreased after changing Me to Ph at the N atom ([**5**]OTf *vs.* [**1**]OTf). Therefore, it was concluded that catalytic activity of azolium-based halogen bond donors is generally determined by the structure of the azolium heterocycle, whereas the substituents on the cycle have significantly less influence on the activity. The experimental data obtained fully agree with the DFT calculations, which themselves had a strong correlation with the ESP distribution data. Therefore, ESP distribution analysis could be successfully employed to predict the catalytic activity of azolium-based XB donors. This experimentally-verified theoretical study highlighted the most promising azolium cycles for applications in organocatalysis.

Conclusion

The results of this study support two major conclusions. First, ESP distribution analysis was successfully implemented to evaluate the relative catalytic activity of a series of structurally similar XB donors. This analysis importantly revealed the strong correlation between the positive electrostatic potential of the σ-hole on the halogen atom and the Gibbs free energy of activation of the considered reactions (*i.e.*, halogen abstraction and carbonyl activation). ESP analysis requires significantly less computational time and energy than computing the localization and energies of reaction transition states; therefore, this study demonstrates a relatively facile method for estimating the relative activity of XB donors. Furthermore, the approach for estimating the relative catalytic activities of azolium catalysts presented herein was confirmed experimentally.

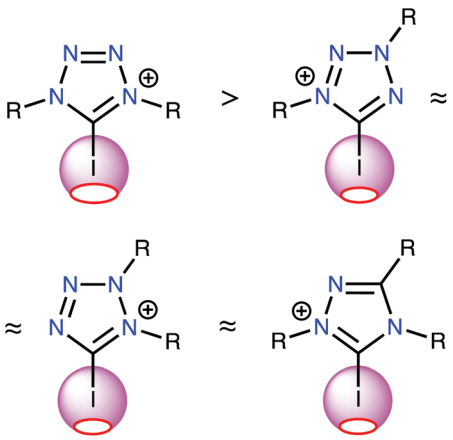

Fig. 5 The most promising azolium-based XB-donating organocatalysts and a relative comparison of their V_s(max) values of the σ-hole on the I atom.

Second, the ESP analysis considering all possible structural types of iodine-containing azolium-based donors that were stable under ordinary conditions unambiguously indicated that the most promising azolium compounds for organocatalysis applications include one 1,2,4-triazolium and three tetrazolium species (Fig. 5). Neither type has been tested in terms of their organocatalytic activities, nor comprehensively described in terms of other properties.

These results can also inspire the rational design and development of new XB-donating organocatalysts comprising the most promising azolium features, without requiring blind screening of the activity of such compounds. Further experimental examinations of similar azolium compounds are ongoing in our laboratory.

Experimental section

Materials and instrumentation

All solvents, 1,3-diketones, hydrazine hydrate, phenylhydrazine, $PhI(OAc)_2$, KOH, MeI, iodine, Na_2SO_4, $MgSO_4$, AgOTf, $NaHCO_3$, $Na_2S_2O_3$, KI, NaOAc, NH_4Cl, 1-methylimidazole, *N*-iodosuccinimide, phenylacetylene, NaN_3, BnBr, and CuI were obtained from commercial sources and used as received. All syntheses were conducted in air. Chromatographic separation was carried out using Macherey-Nagel silica gel 60 M (0.063–0.2 mm). Analytical thin-layer chromatography (TLC) was performed on unmodified Merck ready-to-use plates (TLC silica gel 60 F254) applying UV detection. Melting points (M.p.) were measured on a Stuart SMP30 apparatus in capillaries, and the values reported herein were not corrected. Molar conductivities of ~1×10^{-3} M solutions in MeOH were measured on a Mettler Toledo FE30 conductometer using an Inlab710 sensor. High resolution electrospray ionization time-of-flight mass-spectra (HRESI-TOF-MS) were obtained on a Bruker maXis spectrometer equipped with an electrospray ionization source. The instrument was operated in positive-ion mode with an *m*/*z* range 50–1200. The nebulizer gas flow was 1.0 bar, and the drying gas flow was 4.0 L min^{-1}. For $HRESI^+$-MS, the studied compounds were dissolved in MeOH. Infrared (IR) spectra (4000–400 cm^{-1}) of samples in KBr pellets were recorded on a Shimadzu IR Prestige-21 instrument. ^{1}H- and $^{13}C\{^1H\}$-NMR spectra were measured on a Bruker Avance 400 spectrometer in $CDCl_3$, $(CD_3)_2SO$, CD_3CN, and CD_3OD at 25 °C; the residual solvent signal was used as the internal standard. The NMR monitoring kinetic experiments were carried out by measuring the ^{1}H-NMR spectra every 5 min (four scans; repetition time = 4 s) following the initial equilibration period of 5 min on a Bruker Avance III 500 spectrometer in CD_3OD at 50 °C; the residual solvent signal was used as the internal standard.

X-ray diffraction studies

Crystallographic data for all crystals were obtained using a Rigaku "SuperNova XtaLAB" ([**1**]I, [**5**]I) or a Rigaku "Synergy XtaLAB" ([**5**]OTf) diffractometer, each equipped with a monochromatic micro-focus CuKα X-ray source. All crystals were maintained at 100 K during the data collection. Crystal structures were solved using the ShelXT[69] structure solution program and refined using the ShelXL[70] structure refinement program incorporated in the Olex2[71] program package. Empirical absorption corrections were applied using spherical harmonics implemented in the SCALE3 ABSPACK scaling algorithm (Rigaku Oxford Diffraction, 2020). All crystallographic data for this work can be obtained free of charge from the Cambridge Crystallographic Database (CCDC 2085430 for [**5**]I, 2085431 for [**5**]OTf, 2085432 for [**1**]I).

Analytical and spectroscopic data for [1–5]OTf

The compounds [**1–7**]OTf were characterized by $HRESI^+$-MS, IR, and ^{1}H- and $^{13}C\{^1H\}$-NMR spectroscopies. The compounds [**6**]OTf[72] and [**7**]OTf[73] have been characterized previously, and the description of their synthesis and characterization is in the ESI.†

The $HRESI^+$ mass-spectra of [**1–5**]OTf contain peaks corresponding to the quasi-ions $[M]^+$. The IR spectra of [**1–5**]OTf display one to five weak bands in the range of 3106–2926 cm^{-1}, which were attributed to the C–H stretches. These IR spectra also display one or two medium-to-strong bands in the range of 1648–1457 cm^{-1}, which were attributed to the C=N and C=C stretches. The strong bands corresponding to the stretching frequencies of the S=O and C–F bonds of the triflate anion were observed in the range of 1263–1029 cm^{-1}. In the region of 645–516 cm^{-1} two medium-to-strong bands attributed to the C–I bonds were detected. The ^{1}H-NMR spectra of [**1–5**]OTf contain sets of signals from N–CH_3 and C–CH_3 at 4.24–3.69 and 2.58–2.25 ppm, respectively. The proton resonances from C–C_6H_5 were detected at 7.72–7.06 ppm, whereas the signals from N–C_6H_5 were observed at 7.83–7.68 ppm. The $^{13}C\{^1H\}$-NMR spectra of [**1–5**]OTf displayed the following set of signals: 133.12–129.22 (N–C_6H_5), 131.60–126.05 (C–C_6H_5), 69.22–65.56 (*C*–I), 36.39–35.06 (N–CH_3), and 14.17–12.95 ppm (C–CH_3). Signals from

C=N carbons in the pyrazolium rings were observed at 150.52–148.05 ppm, whereas the signals from the CF_3-group of the triflate anion were detected as a quartet centered around 121.17–120.40 ppm.

Syntheses and characterizations of [1–5]OTf

Syntheses of [1–4]OTf. A solution of hydrazine hydrate (1293 μL, 22.5 mmol) in MeOH (10 mL) was added to a stirred solution of one of the desired 1,3-diketones (15 mmol) in $CHCl_3$ (10 mL). The resulting solution was stirred overnight at RT. The solvent was evaporated *in vacuo* at 50 °C, and the residue was crystallized using hexane (5 mL). The precipitate was filtered off, washed with hexane (10 mL), dried at 50 °C for 2 h in air, and used without additional purification. A solution of the corresponding pyrazole (7 mmol) in CH_2Cl_2 (5 mL) was added to a stirred solution of I_2 (1067 mg, 4.2 mmol) and $PhI(OAc)_2$ (1352 mg, 4.2 mmol) in CH_2Cl_2 (5 mL). The resulting solution was stirred for 1 h at RT. The solvent was evaporated *in vacuo* at 50 °C, and the corresponding 4-iodopyrazole was isolated *via* column chromatography (eluent: EtOAc : hexane = 1 : 1, v/v). A solution of the 4-iodopyrazole (2.5 mmol) in DMSO (2 mL) was added to a stirred solution of KOH (280 mg, 5 mmol) and MeI (233 μL, 3.75 mmol) in DMSO (2 mL). The resulting solution was stirred overnight at RT, and then H_2O (100 mL) was added to the reaction mixture. The product was extracted with EtOAc (3 × 50 mL). The combined organic layers were washed with brine (50 mL), and the organic layer was dried over Na_2SO_4 and filtered from the inorganics. The solvent was evaporated *in vacuo* at 50 °C, and the corresponding 1-methyl-4-iodopyrazole was used without additional purification. A solution of MeI (224 μL, 3.6 mmol) in CH_3CN (1 mL) was added to a stirred solution of the corresponding 1-methyl-3-iodopyrazole (1.2 mmol) in CH_3CN (4 mL). The resulting solution was stirred for 7 d at 85 °C, and the generated precipitate was filtered off, washed with CH_3CN (2 × 3 mL) and Et_2O (1 × 5 mL), and dried at 50 °C for 2 h in air to give the corresponding 1,2-dimethyl-4-iodopyrazolium iodide, which was used without further purification. A solution of AgOTf (136 mg, 0.53 mmol) in MeOH (2 mL) was added to a stirred solution of the corresponding 1,2-dimethyl-4-iodo-pyrazolium iodide (0.53 mmol) in MeOH (3 mL). The suspension was stirred for 15 min at RT, and the precipitate formed was filtered off, washed with MeOH (15 mL), and the combined organic layers were evaporated *in vacuo* at 40 °C. The residue was recrystallized from EtOAc (5 mL) to give [**1–4**]OTf. Yields on the last synthetic step are reported below.

[**1**]OTf: Yield: 83% (176 mg). M.p.: 159–161 °C. Λ_M (CH_3OH, 1.09 × 10^{-3} M): 98.8 Ohm^{-1} cm^{-1} mol^{-1}. ^{1}H-NMR (400.13 MHz, CD_3CN, ppm): δ = 3.93 (s, 6H, N–CH_3), 2.46 (s, 6H, C–CH_3). $^{13}C\{^1H\}$-NMR (101.61 MHz, CD_3CN, ppm): δ = 148.05 (*C*–CH_3), 121.01 (q, $^1J_{CF}$ = 320.7 Hz, *C*F_3), 65.56 (*C*–I), 35.06 (N–*C*H_3), 12.95 (C–*C*H_3). HRMS (ESI-TOF): *m*/*z* calcd for $C_7H_{12}N_2I^+$: 251.0040; found: 251.0042. IR (KBr, selected bands, cm^{-1}): $\tilde{\nu}$ = 3039 (w, C–H), 2926 (w, C–H), 1639 (m, C=N), 1553 (m, C=C), 1509 (w, C=C), 1263 (s, S=O or C–F), 1151 (s, S=O or C–F), 1032 (s, S=O or C–F), 645 (s, C–I), 518 (m–s, C–I).

[**2**]OTf. Yield: 64% (157 mg). M.p.: 137–138 °C. Λ_M (CH_3OH, 9.7 × 10^{-4} M): 239.2 Ohm^{-1} cm^{-1} mol^{-1}. ^{1}H-NMR (400.13 MHz, $CDCl_3$, ppm): δ = 7.66–7.58 (m, 3H, Ph), 7.52–7.49 (m, 2H, Ph), 4.24 (s, 3H, N–CH_3), 4.04 (s, 3H, N–CH_3), 2.62 (s, 3H, C–CH_3). $^{13}C\{^1H\}$-NMR (101.61 MHz, $CDCl_3$, ppm): δ = 150.09, 148.71 (*C*–CH_3, *C*–Ph); 131.60, 129.95, 129.46, 126.05 (Ph); 120.66 (d, $^1J_{CF}$ = 320.7 Hz) 66.25 (*C*–I); 36.39, 35.99 (N–*C*H_3), 13.89 (C–*C*H_3). HRMS (ESI-TOF): *m*/*z* calcd for $C_{12}H_{14}N_2I^+$: 313.0196; found: 313.0198. IR (KBr, selected bands, cm^{-1}): $\tilde{\nu}$ = 3056 (w, C–H), 1503 (m, C=N), 1461 (m, C=C), 1271 (s, C–F), 1260 (s, S=O or C–F), 1153 (s, S=O or C–F), 1030 (s, C–F), 637 (s, C–I), 517 (m, C–I).

[**3**]OTf. Yield: 78% (203 mg). M.p.: 148–149 °C. Λ_M (CH_3OH, 7.3 × 10^{-4} M): 239.2 Ohm^{-1} cm^{-1} mol^{-1}. ^{1}H-NMR (400.13 MHz, $CDCl_3$, ppm): δ = 7.45–7.41 (m, 2H, Ar); 7.11–7.08 (m, 2H, Ar); 4.21 (s, 3H), 4.03 (s, 3H), 3.91 (s, 3H) (N–CH_3, O–CH_3); 2.60 (s, 3H, C–CH_3). $^{13}C\{^1H\}$-NMR (101.61 MHz, $CDCl_3$, ppm): δ = 161.98 (Ar); 150.13, 148.54 (*C*CH_3, *C*–Ar); 131.55, 117.74, 114.92 (Ar); 120.67 (d, $^1J_{CF}$ = 320.5 Hz) 66.41 (*C*–I); 55.54 (O–*C*H_3); 36.36, 35.97 (N–*C*H_3); 13.90 (C–*C*H_3). HRMS (ESI-TOF): *m*/*z* calcd for $C_{13}H_{16}ON_2I^+$: 343.0302; found: 343.0308. IR (KBr, selected bands, cm^{-1}): $\tilde{\nu}$ = 3083 (w, C–H), 3036 (w, C–H), 2966 (w, C–H), 2937 (w, C–H), 2839 (w, C–H), 1613 (s, C=N), 1573 (m, C=C), 1525 (m, C=C), 1460 (m, C=C), 1263 (s, C–F), 1249 (s, S=O or C–F), 1032 (s, S=O or C–F), 641 (s, C–I), 517 (s, C–I).

[**4**]OTf. Yield: 86% (239 mg). M.p.: 175–177 °C. Λ_M (CH_3OH, 8.8 × 10^{-4} M): 261.9 Ohm^{-1} cm^{-1} mol^{-1}. ^{1}H-NMR (400.13 MHz, CD_3OD, ppm): δ = 7.72–7.69 (m, 6H, Ph), 7.65–7.63 (m, 4H, Ph), 4.08 (s, 6H, N–CH_3). ^{13}C NMR (101.61 MHz, CD_3OD, ppm): δ = 150.52 (*C*–Ph); 131.39, 129.88, 129.18 and 126.48 (Ph); 120.40 (d, $^1J_{CF}$ = 318.2 Hz); 66.68 (*C*–I); 35.67 (N–*C*H_3). HRMS (ESI-TOF): *m*/*z* calcd for $C_{17}H_{16}N_2I^+$: 375.0352; found: 375.0361. IR (KBr, selected bands, cm^{-1}): $\tilde{\nu}$ = 3061 (w, C–H), 2961 (w, C–H), 1608 (m, C=N), 1477 (m, C=C), 1457 (m, C=C), 1276 (s, C–F), 1260 (s, S=O or C–F), 1035 (s, S=O or C–F), 640 (s, C–I), 517 (m, C–I).

Synthesis of [5]OTf. A drop of concentrated H_2SO_4 was added to a mixture of phenylhydrazine (600 μL, 6.1 mmol) and acetylacetone (626 μL, 6.1 mmol). The resulting mixture was stirred for 10 min at RT and then treated sequentially with saturated aqueous solutions of $NaHCO_3$ (20 mL), H_2O (20 mL), and brine (20 mL). The organic layer was dried over $MgSO_4$ and then filtered. The solvent was evaporated *in vacuo* at 50 °C to give 3,5-dimethyl-1-phenylpyrazole in 87% yield (915 mg) as a colorless solid, which was used without additional purification. A suspension of 3,5-dimethyl-1-phenylpyrazole (915 mg, 5.32 mmol) in H_2O (2 mL) was added to an aqueous solution (10 mL) of I_2 (2680 mg, 10.55 mmol), KI (5239 mg, 31.56 mmol), and NaOAc (1360 mg, 10 mmol). The resulting suspension was stirred overnight at 60 °C. Then, a saturated aqueous solution of $Na_2S_2O_3$ was gradually added to the reaction mixture until the bright brown color disappeared, at which point, the product was extracted with CH_2Cl_2 (3 × 50 mL).

The combined organic layers were washed with brine (50 mL), and the organic layer was dried over Na_2SO_4 and then

filtered. The solvent was evaporated *in vacuo* at 50 °C to give 3,5-dimethyl-1-phenyl-4-iodopyrazole in 81% yield (1.227 g) as a brown oil, which was used without additional purification. A solution of 3,5-dimethyl-1-phenyl-4-iodopyrazole (988 mg, 3.31 mmol) in MeI (3 mL) was stirred for 3 d at 60 °C, and the precipitate formed was filtered off, washed with Et_2O (10 mL), and dried at 50 °C for 2 h in air to give the 1,3,5-trimethyl-2-phenyl-4-iodopyrazolium iodide in 46% yield (672 mg) as a colorless solid. A solution of AgOTf (118 mg, 0.46 mmol) in MeOH (2 mL) was added to a stirred solution of 1,3,5-trimethyl-2-phenyl-4-iodopyrazolium iodide (203 mg, 0.46 mmol) in MeOH (3 mL). The suspension was stirred for 15 min at RT, and the precipitate formed was filtered off, washed with MeOH (15 mL), and the combined organic layers were evaporated *in vacuo* at 40 °C and recrystallized from EtOAc (5 mL) to give [**5**]OTf as a colorless solid.

[**5**]OTf. Yield: 87% (186 mg). M.p.: 163–164 °C. Λ_M (CH_3OH, 8.2×10^{-4} M): 114.0 Ohm^{-1} cm^{-1} mol^{-1}. ^{1}H-NMR (400.13 MHz, $(CD_3)_2SO$, ppm): 7.83–7.74 (m, 3H, Ph), 7.71–7.68 (m, 2H, Ph), 3.69 (s, 3H, N–CH_3), 2.56 (s, 3H, C–CH_3), 2.23 (s, 3H, C–CH_3). ^{13}C{^{1}H}-NMR (101.61 MHz, $(CD_3)_2SO$, ppm): δ = 149.46, 148.90 (*C*–CH_3); 133.12, 131.95, 131.11, 129.22 (Ph); 121.17 (q, $^1J_{CF}$ = 319.0 Hz, *C*F_3); 69.22 (*C*–I); 36.36 (N–*C*H_3); 14.17, 13.80 (C–*C*H_3). HRMS (ESI-TOF): *m*/*z* calcd for $C_{12}H_{14}N_2I^+$: 313.0196; found: 313.0204. IR (KBr, selected bands, cm^{-1}): $\tilde{\nu}$ = 3106 (w, C–H), 3059 (w, C–H), 3019 (w, C–H), 2938 (w, C–H), 1594 (m, C=N), 1546 (m, C=N), 1504 (s, C=C), 1488 (s, C=C), 1277 (s, C–F), 1260 (s, S=O or C–F), 1224 (s, S=O or C–F), 1031 (s, S=O or C–F), 648 (s, C–I), 517 (m, C–I).

Computational details

Full geometry optimizations of all model structures were carried out *via* DFT calculations with the M06-2X functional[74] using the Gaussian-09 program package.[75] The quasi-relativistic pseudopotential MWB46,[76] which described 46 core electrons, and an appropriate contracted basis set were used for the iodine atoms, and standard 6-31G* basis sets were used for all other atoms. This level of theory was successfully applied by us in studies of very similar metal-free objects and processes.[41,42] No symmetry restrictions were applied during the geometry optimization procedure. The Hessian matrices were calculated analytically for all optimized model structures (i) to confirm the location of the correct minima or saddle points on the potential energy surface (no imaginary frequencies, or one imaginary frequency, respectively) and (ii) to estimate the thermodynamic parameters (calculated at 25 °C) (see Tables S1 and S2 in the ESI†). The molecular surface electrostatic potential calculations were performed using the Multiwfn program (version 3.7)[77] based on the obtained wavefunctions for the optimized equilibrium model structures. The molecular surface electrostatic potentials were visualized in the Chemcraft program (http://www.chemcraftprog.com/). The Cartesian atomic coordinates for all optimized equilibrium model structures are presented in Table S3 in the ESI.†

Conflicts of interest

There are no conflicts to declare.

Acknowledgements

The theoretical calculations and kinetic experiments in this work were supported by the Russian Science Foundation (grant 20-73-10013), and the synthetic portions were supported by the Russian Foundation for Basic Research (grant 19-03-00044). Physicochemical studies were performed at the Center for Magnetic Resonance, Center for X-ray Diffraction Studies, Chemistry Educational Centre, and Center for Chemical Analysis and Materials Research (all at Saint Petersburg State University).

References

1 V. Oliveira, M. Cardoso and L. Forezi, *Catalysts*, 2018, **8**, 605.
2 Y. Qin, L. Zhu and S. Luo, *Chem. Rev.*, 2017, **117**, 9433–9520.
3 D. M. Flanigan, F. Romanov-Michailidis, N. A. White and T. Rovis, *Chem. Rev.*, 2015, **115**, 9307–9387.
4 S. Mondal, S. R. Yetra, S. Mukherjee and A. T. Biju, *Acc. Chem. Res.*, 2019, **52**, 425–436.
5 T. Chanda and J. C. G. Zhao, *Adv. Synth. Catal.*, 2018, **360**, 2–79.
6 S. Vellalath and D. Romo, *Angew. Chem., Int. Ed.*, 2016, **55**, 13934–13943.
7 H. Guo, Y. C. Fan, Z. Sun, Y. Wu and O. Kwon, *Chem. Rev.*, 2018, **118**, 10049–10293.
8 R. Tepper and U. S. Schubert, *Angew. Chem., Int. Ed.*, 2018, **57**, 6004–6016.
9 D. Bulfield and S. M. Huber, *Chem. – Eur. J.*, 2016, **22**, 14434–14450.
10 R. L. Sutar and S. M. Huber, *ACS Catal.*, 2019, **9**, 9622–9639.
11 C. M. Volla, I. Atodiresei and M. Rueping, *Chem. Rev.*, 2014, **114**, 2390–2431.
12 C. Thomas and B. Bibal, *Green Chem.*, 2014, **16**, 1687–1699.
13 M. N. Grayson and K. N. Houk, *J. Am. Chem. Soc.*, 2016, **138**, 9041–9044.
14 M. Puripat, R. Ramozzi, M. Hatanaka, W. Parasuk, V. Parasuk and K. Morokuma, *J. Org. Chem.*, 2015, **80**, 6959–6967.
15 N. Busschaert, C. Caltagirone, W. Van Rossom and P. A. Gale, *Chem. Rev.*, 2015, **115**, 8038–8155.
16 X. Fang and C. J. Wang, *Chem. Commun.*, 2015, **51**, 1185–1197.
17 O. V. Serdyuk, C. M. Heckel and S. B. Tsogoeva, *Org. Biomol. Chem.*, 2013, **11**, 7051–7071.
18 F. E. Held and S. B. Tsogoeva, *Catal. Sci. Technol.*, 2016, **6**, 645–667.

19 X. Han, H. B. Zhou and C. Dong, *Chem. Rec.*, 2016, **16**, 897–906.
20 B. L. Zhao, J. H. Li and D. M. Du, *Chem. Rec.*, 2017, **17**, 994–1018.
21 D. Parmar, E. Sugiono, S. Raja and M. Rueping, *Chem. Rev.*, 2014, **114**, 9047–9153.
22 T. Akiyama and K. Mori, *Chem. Rev.*, 2015, **115**, 9277–9306.
23 T. James, M. van Gemmeren and B. List, *Chem. Rev.*, 2015, **115**, 9388–9409.
24 S. Schindler and S. M. Huber, in *Halogen Bonding II*, ed. P. Metrangolo and G. Resnati, Springer, 2015, pp. 167–204.
25 M. Erdelyi, *Chem. Soc. Rev.*, 2012, **41**, 3547–3557.
26 D. von der Heiden, A. Vanderkooy and M. Erdélyi, *Coord. Chem. Rev.*, 2020, **407**, 213147.
27 S. Benz, A. I. Poblador-Bahamonde, N. Low-Ders and S. Matile, *Angew. Chem., Int. Ed.*, 2018, **57**, 5408–5412.
28 L. Vogel, P. Wonner and S. M. Huber, *Angew. Chem., Int. Ed.*, 2019, **58**, 1880–1891.
29 J. Bamberger, F. Ostler and O. G. Mancheno, *ChemCatChem*, 2019, **11**, 5198–5211.
30 Y. Takeda, D. Hisakuni, C. H. Lin and S. Minakata, *Org. Lett.*, 2015, **17**, 318–321.
31 S. H. Jungbauer, S. M. Walter, S. Schindler, L. Rout, F. Kniep and S. M. Huber, *Chem. Commun.*, 2014, **50**, 6281–6284.
32 J. P. Gliese, S. H. Jungbauer and S. M. Huber, *Chem. Commun.*, 2017, **53**, 12052–12055.
33 M. Kaasik, A. Metsala, S. Kaabel, K. Kriis, I. Jarving and T. Kanger, *J. Org. Chem.*, 2019, **84**, 4294–4303.
34 A. Dreger, E. Engelage, B. Mallick, P. D. Beer and S. M. Huber, *Chem. Commun.*, 2018, **54**, 4013–4016.
35 R. Haraguchi, S. Hoshino, M. Sakai, S. G. Tanazawa, Y. Morita, T. Komatsu and S. I. Fukuzawa, *Chem. Commun.*, 2018, **54**, 10320–10323.
36 K. Torita, R. Haraguchi, Y. Morita, S. Kemmochi, T. Komatsu and S. I. Fukuzawa, *Chem. Commun.*, 2020, **56**, 9715–9718.
37 R. A. Squitieri, K. P. Fitzpatrick, A. A. Jaworski and K. A. Scheidt, *Chem. – Eur. J.*, 2019, **25**, 10069–10073.
38 R. Haraguchi, T. Nishikawa, A. Kanazawa and S. Aoshima, *Macromolecules*, 2020, **53**, 4185–4192.
39 F. Heinen, E. Engelage, A. Dreger, R. Weiss and S. M. Huber, *Angew. Chem., Int. Ed.*, 2018, **57**, 3830–3833.
40 Y. Zhang, J. Han and Z.-J. Liu, *RSC Adv.*, 2015, **5**, 25485–25488.
41 S. N. Yunusova, A. S. Novikov, N. S. Soldatova, M. A. Vovk and D. S. Bolotin, *RSC Adv.*, 2021, **11**, 4574–4583.
42 M. V. Il'in, L. A. Lesnikova, D. S. Bolotin, A. S. Novikov, V. V. Suslonov and V. Y. Kukushkin, *New J. Chem.*, 2020, **44**, 1253–1262.
43 M. V. Il'in and D. S. Bolotin, *Chem. Heterocycl. Compd.*, 2020, **56**, 824–828.
44 M. V. Il'in, A. A. Sysoeva, D. S. Bolotin, A. S. Novikov, V. V. Suslonov, E. V. Rogacheva, L. A. Kraeva and V. Y. Kukushkin, *New J. Chem.*, 2019, **43**, 17358–17366.
45 M. V. Il'in, D. S. Bolotin, V. V. Suslonov and V. Y. Kukushkin, *New J. Chem.*, 2018, **42**, 9373–9376.
46 Y. P. Chang, T. Tang, J. R. Jagannathan, N. Hirbawi, S. Sun, J. Brown and A. K. Franz, *Org. Lett.*, 2020, **22**, 6647–6652.
47 X. Liu and P. H. Toy, *Adv. Synth. Catal.*, 2020, **362**, 3437–3441.
48 R. L. Sutar, E. Engelage, R. Stoll and S. M. Huber, *Angew. Chem., Int. Ed.*, 2020, **59**, 6806–6810.
49 J. Wolf, F. Huber, N. Erochok, F. Heinen, V. Guerin, C. Y. Legault, S. F. Kirsch and S. M. Huber, *Angew. Chem., Int. Ed.*, 2020, **59**, 16496–16500.
50 R. L. Sutar, N. Erochok and S. M. Huber, *Org. Biomol. Chem.*, 2021, **19**, 770–774.
51 Y. Han and H. V. Huynh, *Chem. Commun.*, 2007, 1089–1091, DOI: 10.1039/b615441g.
52 Y. Han, L. J. Lee and H. V. Huynh, *Chemistry*, 2010, **16**, 771–773.
53 Y. Han, H. V. Huynh and G. K. Tan, *Organometallics*, 2007, **26**, 6581–6585.
54 Y. Han and H. V. Huynh, *Dalton Trans.*, 2011, **40**, 2141–2147.
55 S. Yadav, I. Dutta, S. Saha, S. Das, S. K. Pati, J. Choudhury and J. K. Bera, *Organometallics*, 2020, **39**, 3212–3223.
56 S. Saha, S. Yadav, N. U. D. Reshi, I. Dutta, S. Kunnikuruvan and J. K. Bera, *ACS Catal.*, 2020, **10**, 11385–11393.
57 A. Tyagi, N. U. D. Reshi, P. Daw and J. K. Bera, *Dalton Trans.*, 2020, **49**, 15238–15248.
58 A. Peterson, M. Kaasik, A. Metsala, I. Järving, J. Adamson and T. Kanger, *RSC Adv.*, 2019, **9**, 11718–11721.
59 M. Kaasik, S. Kaabel, K. Kriis, I. Järving and T. Kanger, *Synthesis*, 2019, 2128–2135.
60 S. Araki, Y. Wanibe, F. Uno, A. Morikawa, K. Yamamoto, K. Chiba and Y. Butsugan, *Chem. Ber.*, 1993, **126**, 1149–1155.
61 G. Cavallo, J. S. Murray, P. Politzer, T. Pilati, M. Ursini and G. Resnati, *Int. Union Crystallogr. J.*, 2017, **4**, 411–419.
62 T. Clark, M. Hennemann, J. S. Murray and P. Politzer, *J. Mol. Model.*, 2007, **13**, 291–296.
63 P. Politzer and J. Murray, *Crystals*, 2019, **9**, 165.
64 P. Politzer, J. S. Murray, T. Clark and G. Resnati, *Phys. Chem. Chem. Phys.*, 2017, **19**, 32166–32178.
65 M. G. Sarwar, B. Dragisic, L. J. Salsberg, C. Gouliaras and M. S. Taylor, *J. Am. Chem. Soc.*, 2010, **132**, 1646–1653.
66 E. Dimitrijevic, O. Kvak and M. S. Taylor, *Chem. Commun.*, 2010, **46**, 9025–9027.
67 I. Alkorta, G. Sánchez-Sanz and J. Elguero, *CrystEngComm*, 2013, **15**, 3178–3186.
68 N. Momiyama, A. Izumiseki, N. Ohtsuka and T. Suzuki, *ChemPlusChem*, 2021, **86**, 913–919.
69 G. M. Sheldrick, *Acta Crystallogr., Sect. A: Found. Adv.*, 2015, **71**, 3–8.
70 G. M. Sheldrick, *Acta Crystallogr., Sect. C: Struct. Chem.*, 2015, **71**, 3–8.
71 O. V. Dolomanov, L. J. Bourhis, R. J. Gildea, J. A. K. Howard and H. Puschmann, *J. Appl. Crystallogr.*, 2009, **42**, 339–341.
72 W. He, Y. C. Ge and C. H. Tan, *Org. Lett.*, 2014, **16**, 3244–3247.
73 M. Breugst, D. von der Heiden, E. Detmar and R. Kuchta, *Synlett*, 2017, 1307–1313.

74 Y. Zhao and D. G. Truhlar, *Theor. Chem. Acc.*, 2007, **120**, 215–241.

75 M. J. Frisch, G. W. Trucks, H. B. Schlegel, G. E. Scuseria, M. A. Robb, J. R. Cheeseman, G. Scalmani, V. Barone, B. Mennucci, G. A. Petersson, H. Nakatsuji, M. Caricato, X. Li, H. P. Hratchian, A. F. Izmaylov, J. Bloino, G. Zheng, J. L. Sonnenberg, M. Hada, M. Ehara, K. Toyota, R. Fukuda, J. Hasegawa, M. Ishida, T. Nakajima, Y. Honda, O. Kitao, H. Nakai, T. Vreven, J. J. A. Montgomery, J. E. Peralta, F. Ogliaro, M. Bearpark, J. J. Heyd, E. Brothers, K. N. Kudin, V. N. Staroverov, T. Keith, R. Kobayashi, J. Normand, K. Raghavachari, A. Rendell, J. C. Burant, S. S. Iyengar, J. Tomasi, M. Cossi, N. Rega, J. M. Millam, M. Klene, J. E. Knox, J. B. Cross, V. Bakken, C. Adamo, J. Jaramillo, R. Gomperts, R. E. Stratmann, O. Yazyev, A. J. Austin, R. Cammi, C. Pomelli, J. W. Ochterski, R. L. Martin, K. Morokuma, V. G. Zakrzewski, G. A. Voth, P. Salvador, J. J. Dannenberg, S. Dapprich, A. D. Daniels, O. Farkas, J. B. Foresman, J. V. Ortiz, J. Cioslowski and D. J. Fox, *Gaussian 09, Revision C.01*, Gaussian, Inc., Wallingford CT, 2010.

76 A. Bergner, M. Dolg, W. Küchle, H. Stoll and H. Preuß, *Mol. Phys.*, 1993, **80**, 1431–1441.

77 T. Lu and F. Chen, *J. Comput. Chem.*, 2012, **33**, 580–592.